

Variational Graph Generator for Multi-View Graph Clustering

Jianpeng Chen, Yawen Ling, Jie Xu, Yazhou Ren, *Member, IEEE*, Shudong Huang, Xiaorong Pu, Zhifeng Hao, *Senior Member, IEEE*, Philip S. Yu, *Fellow, IEEE*, Lifang He, *Member, IEEE*

Abstract—Multi-view graph clustering (MGC) methods are increasingly being studied due to the explosion of multi-view data with graph structural information. The critical point of MGC is to better utilize the view-specific and view-common information in features and graphs of multiple views. However, existing works have an inherent limitation that they are unable to concurrently utilize the consensus graph information across multiple graphs and the view-specific feature information. To address this issue, we propose Variational Graph Generator for Multi-View Graph Clustering (VGMGC). Specifically, a novel variational graph generator is proposed to extract common information among multiple graphs. This generator infers a reliable variational consensus graph based on a priori assumption over multiple graphs. Then a simple yet effective graph encoder in conjunction with the multi-view clustering objective is presented to learn the desired graph embeddings for clustering, which embeds the inferred view-common graph and view-specific graphs together with features. Finally, theoretical results illustrate the rationality of VGMGC by analyzing the uncertainty of the inferred consensus graph with information bottleneck principle. Extensive experiments demonstrate the superior performance of our VGMGC over SOTAs.

Index Terms—Multi-view graph clustering, graph generator, graph learning, variational inference, information bottleneck.

I. INTRODUCTION

ATTRIBUTED graph clustering has received increasing attention with the development of graph structure data, such as social networks, academic networks, and world wide web [1, 2, 3]. Attributed graph clustering aims to better analyze the graphs with its attributed features for clustering task, which can benefit lots of fields such as product recommendation [4] and community detection [5]. On the other hand, many of graph structure data contain multiple views in real-world applications, for example, graphs in social networks can be constructed based on common interests or

followers of users, and graphs in academic networks can be established by co-authors or citations of papers. Therefore, lots of multi-view graph clustering (MGC) methods have emerged in recent years for better mining the information of multi-view graphs [6, 7, 8].

Generally, MGC methods could be categorized into two types [7, 9, 10, 11]. One type generates a global affinity matrix of all samples for all views and then groups them into different clusters [9, 12, 13, 14]. These methods successfully demonstrate the effectiveness of learning a consensus graph for analyzing all views. Another type learns representations for individual views via graph embedding techniques, and then incorporates them into global representations. Subsequently, traditional clustering methods, such as k -means [15], can be adopted to obtain clustering results [6]. Benefitting from the graph embedding ability of Graph Neural Networks (GNNs) [3, 16, 17, 18], the two types of methods have been largely improved [6, 7, 19, 20]. Nevertheless, both studies have inherent limitations. For the first type of works, the consensus graph reflects the common topological information of all views. But if we directly partition the consensus graph, the latent view-specific information in features will be ignored. As for the second type of works, each view's graph embeddings are learned separately, so the global topological information might be ignored. Therefore, it is desirable to develop a method that is able to assimilate both the view-common and view-specific topological information, and at the mean time, embed the feature information by utilizing the superior graph embedding ability of GNNs.

To achieve the above goal, we will have two major challenges: 1) how to explore the consensus information and utilize it to generate a consensus graph that is applicable to GNNs, and 2) how to design a GNN that could embed the view-specific information and the generated consensus graph into features together. Considering the first issue, the generated consensus graph requires some properties. First, it must imply the *common information* from both features and graphs. Second, if there is an observed graph that is unreliable, it should depend less on this unreliable graph, in other words, different graphs have different probabilities to be employed for generating the consensus graph. This property requires that we infer the consensus graph *with a specific probability*. Third, it should be *sparse* to avoid large storage and computation consumption, and meanwhile to improve the robustness [21, 22]. Based on these concerns,

(Corresponding author: Yazhou Ren)

Jianpeng Chen, Yawen Ling, Jie Xu, Yazhou Ren, and Xiaorong Pu are with the School of Computer Science and Engineering, University of Electronic Science and Technology of China, Chengdu 611731, China (e-mail: {cjpcool, yawen.Ling, jiexuwork}@outlook.com; {yazhou.ren, puxiao}@uestc.edu.cn).

Shudong Huang is with the College of Computer Science, Sichuan University, Chengdu 610065, China (e-mail: huangsd@scu.edu.cn).

Zhifeng Hao is with the Department of Mathematics, the College of Science, Shantou University, Shantou 515063, China (e-mail: haozhifeng@stu.edu.cn).

Philip S. Yu is with the Department of Computer Science, University of Illinois at Chicago, Chicago, IL 60607 USA (e-mail: psyu@cs.uic.edu).

Lifang He is with the Department of Computer Science and Engineering, Lehigh University, PA 18015, USA (e-mail: lih319@lehigh.edu).

the technique of variational inference is a perfect match, which could infer sparse and discrete variables with a specific probability. More importantly, with our novel design, the proposed variational graph generator can extract the common information among multiple graphs and global features, as well as some task relevant information. Specifically, we first propose a priori assumption over multi-graphs, and then design a variational graph generator to infer a sparse consensus graph from global features based on this priori assumption (see Section III-C). As to the second issue, the previous researches about GNNs [3, 22, 23] have suggested that lots of parameters in GNNs are redundant, and the powerful representation ability of GNNs comes from the message passing process. To this end, we design a simple yet effective encoder with a parameter-free message-passing method to embed the view-specific and view-common graph information together (see Section III-D). In addition, we introduce our multi-view fusion method to incorporate graph embeddings from all views (see Section III-E). Finally, our objective functions are proposed to optimize the model for the multi-view clustering task (see Section III-F). For brevity, we call the proposed approach VGMGC (Variational Graph Generator for Multi-View Graph Clustering). Furthermore, we have theoretically analyzed the rationality of the generated graph (see Section III-G), and empirically demonstrated the effectiveness of VGMGC (see Section IV). The main contributions of this work include:

- We propose a novel variational graph generator based on a priori assumption over multi-graphs, which can generate a variational consensus graph with the required properties from global features for GNNs. To the best of our knowledge, this work is the first trial utilizing variational inference to infer a discrete graph for multi-view graph learning.
- We propose a simple yet effective encoder to embed the consensus graph and view-specific graphs into embeddings, in a parameter-free message-passing manner.
- Theoretical analysis illustrates the rationality of the inferred consensus graph and our proposals. Experiments on eight widely-used datasets demonstrate the superior performance of our method compared with SOTAs.

II. RELATED WORKS

A. Graph Neural Networks for Multi-View Graph Clustering

Ren et al. [24] reviewed some methods for deep multi-view clustering, such as dual self-paced multi-view clustering [25], self-supervised discriminative feature learning for deep multi-view clustering [26], and unsupervised deep embedding for clustering analysis [27], but the issues in multi-view graph clustering still remain to be explored. Xu et al. [23] has theoretically proved that GNNs can efficiently embed graph structural information with features. Promoted by the success of GNNs, several multi-view clustering methods have emerged. Specifically, Fan et al. [7] first employed GNN [16] for MGC. It selects an informative graph with features and conducts GNN to generate embeddings for clustering, and multi-view information is injected by backpropagation. However, the information implied in unselected graphs are largely

lost by this way. Cheng et al. [6] adopted GNN on multiple features with a shared graph, but it cannot be generalized to the data with multiple graphs. Alternatively, researchers in [19] and [20] embedded each graph's information in each view separately via graph filter, and then learned a consensus graph which will be partitioned to different clusters. However, due to their clustering results only being determined by the generated graph, some useful information in features is ignored. Recently, Liu et al. [28] proposed stationary diffusion state neural estimation (SDSNE) for multi-view clustering, which utilizes the stationary diffusion to get a consensus graph, and performs the spectral clustering on this graph directly. However, in essence, SDSNE belongs to the first type, so it also suffers from the inherent issues of this type, *i.e.*, the clustering results determined by the consensus graph, and some feature information is lost. Differently, the proposed VGMGC could reserve useful feature information, and utilize the powerful graph embedding ability of GNNs to assimilate both the consensus and specific graph information for clustering task.

B. Variational Inference for Multi-View Graph Clustering

Kingma and Welling [29] proposed variational autoencoders (VAE), which has subsequently influenced lots of fields. For example, Dilokthanakul et al. [30] introduced VAE for clustering task. Xu et al. [31] disentangled view-specific and view-common information via VAE for multi-view clustering task. In the field of graph clustering, Kipf and Welling [32] first adopted this technique to graph representation learning for link prediction. Following this work, Pan et al. [33] proposed a variational adversarial approach to learn a robust graph embedding. Sun et al. [34] extended graph VAE to infer stochastic node representations. However, all these works aim at inferring the node representations rather than a graph.

It seems hard to utilize variation to infer a graph since the observed graph is certain and prior distribution of the graph is unknown. Even so, a few works have tried to infer a graph. Luo et al. [35] introduced a prior to graph, and sampled a new graph from observed one via uniform distribution. However, this graph is not essentially a generated one, but only a subgraph of the observed graph. Elinas et al. [36] introduced two hyper-parameters to control the uncertainty of a graph, and generated a graph based on variational inference and k -nearest neighbors (kNN), but it also has two potential issues. First, the selection of the two hyper-parameters is groundless. Second, its variational ability is largely restricted by kNN, and the k in kNN is hard to set. Differently, in the proposed variational graph generator, the uncertainty is dependent on how reliable the observed graphs are for the clustering task. Therefore, the inferred graph is more robust and task-related. Moreover, to the best of our knowledge, this is the first trial to infer a graph for multi-view clustering task.

III. METHODS

A. Problem Statement

Given multiple graphs with their attributed features $\{\mathcal{G}^v = (\mathbf{X}^v, \mathbf{A}^v)\}_{v=1}^V$, where $\mathbf{X}^v \in \mathbb{R}^{n \times d_v}$ denotes the features of n nodes in the graph of the v -th view, and $\mathbf{A}^v = \{a_{ij} \mid a_{ij} \in$

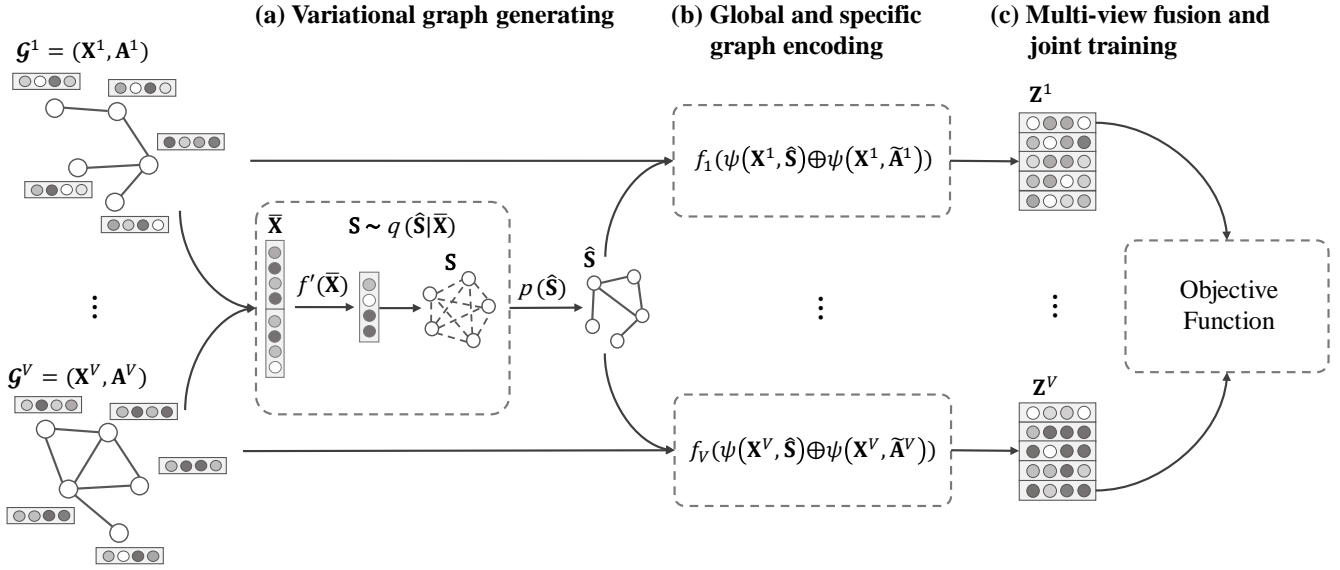


Fig. 1. The illustration of VGMGC. \oplus denotes concatenating operation. We first infer a cross-view consensus graph $\hat{\mathbf{S}}$ via the variational graph generator, and then, the variational consensus graph is normalized, and we feed it with each attributed view-specific graph into the graph encoder, which could generate latent features \mathbf{Z}^v for each view. Finally, all views' latent features are weighted and concatenated for training and clustering.

$\{0, 1\}$ denotes the corresponding adjacency matrix (with self-loop), respectively, MGC aims to partition the n samples into c clusters. Let a diagonal matrix \mathbf{D}^v (where $\mathbf{D}_{ii}^v = \sum_j a_{ij}^v$) represent the degree matrix of \mathbf{A}^v , the normalized adjacent matrix is defined as $\tilde{\mathbf{A}}^v = (\mathbf{D}^v)^{-1} \mathbf{A}^v$. We define $\bar{\mathbf{X}} \in \mathbb{R}^{n \times d'}$ as a global feature shared by all views. Generally, if the dataset does not contain this feature, it is generated by concatenating $\{\mathbf{X}^v\}_{v=1}^V$, i.e., $\bar{\mathbf{X}} = \text{Concat}(\mathbf{X}^1, \mathbf{X}^2, \dots, \mathbf{X}^V)$ where $\text{Concat}(\cdot, \cdot)$ denotes concatenating operation. Specifically, let $\bar{\mathbf{Z}} \in \mathbb{R}^{n \times (V \cdot D)}$ and $\mathbf{Z}^v \in \mathbb{R}^{n \times D}$ be the global and each view's latent representation respectively. The goal of this work is to learn better MGC by leveraging the novel variational graph generator and an effective graph encoder. The overall descriptions of notations are shown in Appendix A.

B. Overview of Variational Graph Generator for Multi-View Graph Clustering

The overview of VGMGC is shown in Figure 1. In the following, we will concentrate on three questions to disassemble our proposed framework: a) how the variational consensus graph is inferred from multi-view graph data (see Section III-C), b) how the variational consensus graph is incorporated with each view's specific graph and features to generate latent feature \mathbf{Z}^v (see Section III-D), and c) how to fuse multi-view latent features for collaborative training and clustering (see Section III-E).

C. Variational Graph Generator

We first present our variational graph generator, which can infer a discrete consensus graph containing the common feature information as well as common topological information simultaneously, and we will introduce how the two kinds of common information are captured in each step. On top of that, another difference between our variational graph generator and

previous VAEs [29, 30, 31, 32] is that we aim at inferring a discrete graph directly, but previous VAEs are to infer latent embeddings of nodes and construct the graph by computing the similarities between these embeddings.

Let $\hat{\mathbf{S}} = \{\hat{s}_{ij} \mid \hat{s}_{ij} \in \{0, 1\}\}$ be an independent consensus graph. We aim to model the multi-graph data $\{\mathbf{A}^v\}_{v=1}^V$ to find a better consensus graph, i.e., $\hat{\mathbf{S}}$. Therefore, this generative model tries to learn the joint distribution:

$$p(\mathbf{X}^v, \hat{\mathbf{S}}, \mathbf{A}^v) = p(\mathbf{A}^v \mid \mathbf{X}^v, \hat{\mathbf{S}})p(\mathbf{X}^v, \hat{\mathbf{S}}), \quad (1)$$

where $p(\mathbf{X}^v, \hat{\mathbf{S}}, \mathbf{A}^v)$ represents the joint probability of \mathbf{X}^v , $\hat{\mathbf{S}}$, and \mathbf{A}^v .

1) *A Priori Assumption Over Multi-Graph*: The priori assumption could not only give the consensus graph a definition, but also inject some task-relevant information and consensus information among graphs into the consensus graph.

Begin with the definition of this graph, we consider that the consensus graph is a Gilbert random graph [37], where the edges in $\hat{\mathbf{S}}$ are conditionally independent with each other, so the probability of generating $\hat{\mathbf{S}}$ could be factorized as:

$$p(\hat{\mathbf{S}}) = \prod_{i,j} p(\hat{s}_{ij}).$$

An evident instantiation of $p(\hat{s}_{ij})$ is the Bernoulli distribution, i.e., $\hat{s}_{ij} \sim \text{Bern}(\beta_{ij})$. $p(\hat{s}_{ij} = 1) = \beta_{ij}$ is the prior probability of whether there exists an edge between nodes i and j , where β are parameters determined by all observed graphs $\{\mathbf{A}^v\}_{v=1}^V$ with their corresponding optimizable beliefs $\{b^v\}_{v=1}^V$. The belief $b^v \in (0, 1]$ of \mathbf{A}^v , which could be obtained by a self-supervised method (which will be introduced in Section III-E), is to control how much the v -th graph should be trusted for our clustering task. Then, we aggregate all graphs $\{\mathbf{A}^v\}_{v=1}^V$

with their corresponding beliefs $\{b^v\}_{v=1}^V$ by computing the consensus among them to learn the prior parameter β :

$$\beta_{ij} = \frac{\sum_v [b^v \cdot a_{ij}^v + (1 - b^v) \cdot (1 - a_{ij}^v)]}{\sum_v b^v}. \quad (2)$$

From Eq. (2), the belief (or task relevance β) of each graph and the consensus among the multiple graphs can be injected into the consensus graph. This conclusion is also proved in Theorems 1 and 2.

2) *Inference Process*: In the inference process, the variational graph generator tries to capture the common feature information from global features by computing the posterior probability.

Specifically, the variational consensus graph $\hat{\mathbf{S}}$ is generated from global features $\bar{\mathbf{X}}$, so the posterior of $\hat{\mathbf{S}}$ could be written as $p(\hat{\mathbf{S}} | \bar{\mathbf{X}})$. However, considering the posterior is intractable to be calculated [29, 30], we propose a neural network which is based on self-attention [38] to approximate it, *i.e.*, $q_{\phi'}(\hat{\mathbf{S}} | \bar{\mathbf{X}})$ where ϕ' denotes the trainable parameters of the neural network. The proposed neural network could be written as:

$$\alpha = \mathbf{K}\mathbf{Q}^T, \text{ where } \mathbf{K} = f'(\bar{\mathbf{X}}), \mathbf{Q} = \mathbf{K}\mathbf{W}, \quad (3)$$

where $\alpha = \{\alpha_{ij}\} \in \mathbb{R}^{n \times n}$ denotes the neurons used to obtain variable $\hat{\mathbf{S}}$, f' represents a multilayer perceptron (MLP), and \mathbf{W} is the trainable parameters. Therefore, ϕ' contains trainable parameters in f' and \mathbf{W} .

Moreover, due to the structural information α needs to reserve the important information of global features $\bar{\mathbf{X}}$, we are expected to maximize the mutual information between α and $\bar{\mathbf{X}}$, *i.e.*, $I(\alpha, \bar{\mathbf{X}})$. However, maximizing $I(\alpha, \bar{\mathbf{X}})$ is intractable, we achieve this by maximizing its lower bound.

In doing so, from Eq. (3), we can know that the information in α is deterministic given \mathbf{K} and \mathbf{Q} . So, we have:

$$\arg \max I(\alpha, \bar{\mathbf{X}}) \cong \arg \max I(\mathbf{K}, \bar{\mathbf{X}}) \text{ and } \arg \max I(\mathbf{Q}, \bar{\mathbf{X}}).$$

Considering the three variables \mathbf{K} , \mathbf{Q} and $\bar{\mathbf{X}}$, we have the Markov chain: $\bar{\mathbf{X}} \rightarrow \mathbf{K} \rightarrow \mathbf{Q}$. According to Data Processing Inequality, we can get $I(\mathbf{K}, \bar{\mathbf{X}}) \geq I(\mathbf{Q}, \bar{\mathbf{X}})$. This demonstrates that $I(\mathbf{Q}, \bar{\mathbf{X}})$ is the lower bound of $I(\mathbf{K}, \bar{\mathbf{X}})$, and we have:

$$\arg \max I(\mathbf{K}, \bar{\mathbf{X}}) \text{ and } \arg \max I(\mathbf{Q}, \bar{\mathbf{X}}) \cong \arg \max I(\mathbf{Q}, \bar{\mathbf{X}}).$$

By concluding the two equations above, we obtain Eq. (4):

$$\arg \max_{\phi'} I(\alpha, \bar{\mathbf{X}}) \cong \arg \max_{\phi'} I(\mathbf{Q}, \bar{\mathbf{X}}). \quad (4)$$

Eq. (4) enforces the posterior probability to reserve as more global feature information as possible.

On the other hand, due to the discrete nature of graph $\hat{\mathbf{S}}$, we adopt reparameterization trick to optimize these parameters with gradient-based methods [39]. In this work we utilize binary concrete distribution for relaxation, *i.e.*, $s_{ij} \sim \text{BinConcrete}(\alpha_{ij}, \tau)$, where $\tau > 0$ and α_{ij} represent the temperature and location parameters respectively. Specifically, let variable $U \sim \text{Uniform}(0, 1)$, the relaxed weight $s_{ij} \in (0, 1)$ of edge (i, j) is calculated as:

$$q_{\phi'}(\hat{s}_{ij} | \bar{\mathbf{x}}) = \sigma((\log U - \log(1 - U) + \alpha_{ij})/\tau), \quad (5)$$

with $U \sim \text{Uniform}(0, 1)$,

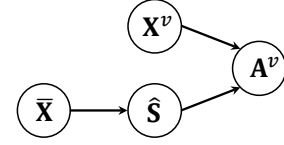


Fig. 2. The Bayesian net of our variational graph generator about variables: \mathbf{A}^v , $\hat{\mathbf{S}}$, $\bar{\mathbf{X}}$ and \mathbf{X}^v .

where $\sigma(\cdot)$ denotes the *Sigmoid* function. It is easy to demonstrate the rationality of using the binary concrete distribution of s_{ij} to approximate the priori Bernoulli distribution of \hat{s}_{ij} [40].

3) *Generative Process*: The generative process can enhance the common topological information among multiple graphs by reconstructing every graph. Concretely, after obtaining the latent consensus graph $\hat{\mathbf{S}}$, in the generative process, we model all views' graphs $\{\mathbf{A}^v\}_{v=1}^V$ in a collaborative manner. Let $\{\xi^v\}_{v=1}^V$ be the learnable parameters of decoder, the likelihood of v -th graph is as follow:

$$\check{\mathbf{A}}^v = p_{\xi^v}(\mathbf{A}^v | \mathbf{X}^v, \hat{\mathbf{S}}). \quad (6)$$

4) *Evidence Lower Bound*: According to Jensen's inequality and our Bayesian net (Figure 2), it is easy to prove that maximizing the likelihood of observed graphs (*i.e.*, $p(\mathbf{A}^v)$) is equal to maximizing the evidence lower bound (ELBO):

$$\begin{aligned} \sum_{v=1}^V \log p(\mathbf{A}^v) &= \sum_{v=1}^V \log \int \int p(a^v, \hat{s}, x^v) d\hat{s} dx^v \\ &= \sum_{v=1}^V \log \int \int \frac{q(\hat{s} | \bar{x})}{q(\hat{s} | \bar{x})} p(a^v, \hat{s}, x^v) d\hat{s} dx^v \\ &= \sum_{v=1}^V \log \int \mathbb{E}_{q(\hat{s} | \bar{x})} \frac{p(a^v, \hat{s}, x^v)}{q(\hat{s} | \bar{x})} dx^v \\ &\geq \sum_{v=1}^V \mathbb{E}_{q(\hat{s} | \bar{x})} \log \int \frac{p(a^v, \hat{s}, x^v)}{q(\hat{s} | \bar{x})} dx^v, \text{ (Jensen's inequality),} \\ &= \sum_{v=1}^V \mathbb{E}_{q(\hat{s} | \bar{x})} \log \int \frac{p(a^v | \hat{s}, x^v) p(\hat{s})}{q(\hat{s} | \bar{x})} p(x^v) dx^v, \text{ } (\hat{s} \perp x^v | \emptyset), \\ &\geq \sum_{v=1}^V \mathbb{E}_{q(\hat{s} | \bar{x}) p(x^v)} \log p(a^v | \hat{s}, x^v) + \mathbb{E}_{q(\hat{s} | \bar{x})} \log \frac{p(\hat{s})}{q(\hat{s} | \bar{x})} \\ &= \sum_{v=1}^V \mathbb{E}_{q(\hat{s} | \bar{x}) p(x^v)} \log p(a^v | \hat{s}, x^v) - KL(q(\hat{s} | \bar{x}) || p(\hat{s})). \end{aligned}$$

Here, $\hat{s} \perp x^v | \emptyset$ is derived from the Bayesian net (Figure 2). Therefore, our first objective function, *i.e.*, ELBO, can be written as:

$$\begin{aligned} \arg \max_{\phi', \{\xi^v\}_{v=1}^V} \mathcal{L}_E &= \sum_{v=1}^V \mathbb{E}_{q_{\phi'}(\hat{\mathbf{S}} | \bar{\mathbf{X}}) p(\mathbf{X}^v)} \left[\log p_{\xi^v}(\mathbf{A}^v | \hat{\mathbf{S}}, \mathbf{X}^v) \right] \\ &\quad - KL(q_{\phi'}(\hat{\mathbf{S}} | \bar{\mathbf{X}}) || p(\hat{\mathbf{S}})). \end{aligned} \quad (7)$$

The first term of Eq. (7) is the expectation of the conditional likelihood over the approximate posterior, *i.e.*, expected log likelihood (ELL), and the second term is the KL divergence between the approximate posterior of the variational consensus

graph and its prior. Under our priori assumption, *i.e.*, $p(s_{ij}) = \text{Bern}(\beta_{ij})$, the KL divergence is bounded:

$$\begin{aligned} KL(q_{\phi'}(\hat{\mathbf{S}} | \bar{\mathbf{X}}) \| p(\hat{\mathbf{S}})) &= -H(q_{\phi'}(\hat{\mathbf{S}})) + \sum_{ij} \log \frac{1}{\beta_{ij}} \\ &\leq \sum_{ij} \log \frac{1}{\beta_{ij}}, \end{aligned} \quad (8)$$

where $H(\cdot)$ denotes entropy and β is determined by the observed graphs and corresponding beliefs (see Eq. (2)). From this bound, we can know that the maximum variational information in the variational consensus graph is dependent on the consistency of these observed graphs and how relative they are to our clustering task. For example, when all graphs are consistent with $\{a_{ij}^v = 1\}_{v=1}^V$, we could get $\log \beta_{ij} = 1$, which enforces $H(q(\hat{s}_{ij})) = 0$.

D. Global and Specific Graph Encoding

In this section, we will propose our graph encoder, which contains three inputs, *i.e.*, observed graph data \mathbf{A}^v with its attributed features \mathbf{X}^v , and a variational consensus graph $\hat{\mathbf{S}}$. The aim of this graph encoder is to inject the consensus graph structure information into each specific view and generate embeddings. So this module could be decomposed into two steps: 1) message-passing-based graph embedding (denoted by $\psi(\cdot)$) to embed the specific and consensus graph structure respectively; 2) low-dimensional representation learning (denoted by $f_v(\cdot)$) to fuse the view-specific graph embeddings and consensus graph embeddings while obtaining a lower-dimensional representations.

1) *Message-Passing-Based Graph Embedding*: Inspired by previous GNNs [3, 18, 41], we remove most redundant parameters in GNNs and introduce a simple yet effective message-passing method in this part.

Let $\mathbf{E}^{(l)}$ be the embedding of l -th layer, the definition of vanilla GNN [16] is as follow:

$$\mathbf{E}^{(l+1)} = (\tilde{\mathbf{A}}\mathbf{E}^{(l)}\mathbf{W}^{(l)}), \text{ where } \mathbf{E}^{(0)} = \mathbf{X}.$$

We first remove the unnecessary parameters \mathbf{W} from this equation, and then, add a residual connection to every layer from the input features \mathbf{X} . Therefore, the improved parameter-free graph neural network could be written as:

$$\mathbf{E}^{(l+1)} = \tilde{\mathbf{A}}\mathbf{E}^{(l)} + \mathbf{X}.$$

Finally, we can obtain our message-passing method via mathematical induction:

$$\psi(\mathbf{X}, \tilde{\mathbf{A}}) = \left(\sum_{l=0}^{\text{order}} \tilde{\mathbf{A}}^l + \mathbf{I} \right) \mathbf{X}, \quad (9)$$

where *order* is a hyper-parameter which denotes the aggregation orders on graph \mathbf{A} , and \mathbf{I} denotes the identity matrix. $\tilde{\mathbf{A}}$ and \mathbf{X} are normalized graphs and their attributed features, respectively.

2) *Low-Dimensional Representation*: A straightforward instantiation of $f_v(\tilde{\mathbf{A}}, \hat{\mathbf{S}}, \mathbf{X})$ is MLP. Concretely, we concatenate the specific graph embeddings and consensus graph embeddings and feed them into this MLP to get a lower-dimensional embeddings $\mathbf{Z}^v \in \mathbb{R}^{n \times D}$:

$$\begin{aligned} \mathbf{Z}^v &= f_v(\tilde{\mathbf{A}}^v, \hat{\mathbf{S}}, \mathbf{X}^v) \\ &= f_v(\text{Concat}(\psi(\mathbf{X}^v, \tilde{\mathbf{A}}^v), \psi(\mathbf{X}^v, \hat{\mathbf{S}}))), \end{aligned} \quad (10)$$

Here, the propagation of \mathbf{X}^v over ψ and f_v will lead to some information loss. To reserve more view-specific feature information, we maximize the mutual information $I(\mathbf{X}^v, \mathbf{Z}^v)$:

$$\arg \max_{\phi^v} I(\mathbf{Z}^v, \mathbf{X}^v), \quad (11)$$

where ϕ^v represents the learnable parameters in f_v .

E. Multi-View Fusion for Clustering Task

1) *Multi-View Fusion*: To fuse all views' embeddings $\{\mathbf{Z}^v\}_{v=1}^V$, we first assign beliefs $\{b^v\}_{v=1}^V$ to every view. Intuitively, these beliefs indicate how the corresponding view is relative to our clustering task. Then, we reweight every view via its belief, and concatenate them to get final global representations $\bar{\mathbf{Z}} \in \mathbb{R}^{n \times (V \cdot D)}$. This process could be formulated as:

$$\bar{\mathbf{Z}} = \text{Concat}(b^1 \mathbf{Z}^1, b^2 \mathbf{Z}^2, \dots, b^V \mathbf{Z}^V). \quad (12)$$

This global representation $\bar{\mathbf{Z}}$ is then fed into k -means for clustering. Therefore, how to find correct belief for each view is crucial. To this end, we propose a self-supervised strategy. We first initialize all beliefs to 1, *i.e.*, $\{b^{(0),v} | b^{(0),v} = 1\}_{v=1}^V$, where $b^{(0),v}$ denotes the initial belief of v -th view, then, we generate $\bar{\mathbf{Z}}^{(t-1)}$ via Eq. (12) and conduct k -means on it to obtain the pseudo-labels of t -th epoch. Meanwhile, each view's predicted labels are also obtained by k -means. After that, we consider the pseudo-labels from $\bar{\mathbf{Z}}^{(t-1)}$ as ground-truth and other predicted labels from $\{\mathbf{Z}^v\}_{v=1}^V$ as prediction results to compute each view's clustering score (like normalized mutual information), *i.e.*, $\text{score}^{(t),v}$. These scores are normalized for updating beliefs:

$$b^{(t),v} = \left(\frac{\text{score}^{(t),v}}{\max(\text{score}^{(t),1}, \text{score}^{(t),2}, \dots, \text{score}^{(t),V})} \right)^\rho, \quad (13)$$

where $\rho \geq 0$ is a soft parameter. When $\rho = 0$, we can get $b^{(t),v} = 1$ for all t and v , which denotes that all graphs are equally believed; when $\rho \rightarrow \infty$, $\{b^{(t),v}\}_{v=1}^V$ are binarized. Finally, we can generate $\bar{\mathbf{Z}}^{(t)}$ via Eq. (12) under the new beliefs $\{b^{(t),v}\}_{v=1}^V$, which will be utilized to train the model and generate a more correct belief in next epoch.

2) *Multi-View Clustering Loss*: The clustering loss is widely used in traditional clustering task [6, 27, 42], which encourages the assignment distribution of samples in the same cluster being more similar. Concretely, let Q^v be a soft assignment calculated by Student's t -distribution [43] of v -th view, and P^v be a target distribution calculated by sharpening the soft assignment Q^v . For MGC, we encourage

each view's soft distribution to fit the global representation's target distribution by KL divergence:

$$\mathcal{L}_c = \sum_{v=1}^V KL(\bar{P}||Q^v) + KL(\bar{P}||\bar{Q}), \quad (14)$$

where \bar{P} and \bar{Q} denote the target and soft distribution of global representation $\bar{\mathbf{Z}}$.

F. Objective Function

Our objective function contains three parts: maximizing ELBO (\mathcal{L}_E) to optimize the variational graph generator; maximizing mutual information ($I(\mathbf{Z}^v, \mathbf{X}^v)$ and $I(\mathbf{Q}, \bar{\mathbf{X}})$) to preserve feature information; and minimizing clustering loss (\mathcal{L}_c) to optimize the task-related clustering results. γ_c and γ_E are introduced to trade off the numerical value of \mathcal{L}_c and \mathcal{L}_E . Formally, we have the objective function:

$$\arg \min_{\phi', \eta', \{\phi^v\}_{v=1}^V, \{\eta^v\}_{v=1}^V} \mathcal{L}_r + \gamma_c \mathcal{L}_c - \gamma_E \mathcal{L}_E. \quad (15)$$

Here, \mathcal{L}_r is an instantiation of negative lower bound of $I(\mathbf{Z}^v, \mathbf{X}^v)$ and $I(\alpha, \bar{\mathbf{X}})$ (see Section III-G3), and $\{\eta^v\}_{v=1}^V$ and η' denote corresponding learnable parameters. Notably, the parameters of $p_{\xi^v}(\mathbf{A}^v | \hat{\mathbf{S}}, \mathbf{X}^v)$ and f_v are shared in our model, so $\{\xi^v\}_{v=1}^V$ is omitted in Eq. (15). More implementation details of each term can be found in Appendix C.

G. Theoretical Analysis

In this subsection, we propose two theorems for demonstrating that the consensus and task relevance are implied in the generated consensus graph at first (see Section III-G1). Then, we introduce the variational graph information bottleneck (\mathcal{IB}_{graph}), and prove the connection between our objective function with \mathcal{IB}_{graph} . This can further explain what kind of information is learnt by the consensus graph (see Section III-G2). Finally, we compute the lower bound of mutual information to optimize the proposed $I(\mathbf{Z}^v, \mathbf{X}^v)$ and $I(\alpha, \bar{\mathbf{X}})$ (see Section III-G3).

1) *Uncertainty of Consensus Graph*: Let $H(\hat{\mathbf{S}})$ denote the uncertainty of $\hat{\mathbf{S}}$, and $d_{Ham}(\mathbf{A}^1, \mathbf{A}^2)$ denote the Hamming distance, which quantizes the inconsistency of graph \mathbf{A}^1 and \mathbf{A}^2 . We have the following theorems:

Theorem 1 (Consensus among graphs). *Assume all graphs are equally reliable, the more consistent the observed graphs are, the less uncertain the consensus graph is, and vice versa:*

$$H(\hat{\mathbf{S}}) \propto d_{Ham}(\mathbf{A}^1, \mathbf{A}^2). \quad (16)$$

Proof. Assume there are two views with equal belief, i.e., $V = 2$ and $b^1 = b^2 = b$, we have:

$$\log \beta_{ij} = \log \frac{b(a_{ij}^1 + a_{ij}^2) + (1-b)(2 - (a_{ij}^1 + a_{ij}^2))}{2b}.$$

Note that KL divergence is always positive, so we have :

$$\begin{aligned} KL(q_{\phi'}(\hat{\mathbf{S}} | \bar{\mathbf{X}}) || p(\hat{\mathbf{S}})) &= -H(\hat{\mathbf{S}}) + \sum_{ij} \log \frac{1}{\beta_{ij}} \geq 0 \\ \Rightarrow H(\hat{\mathbf{S}}) &\leq \sum_{ij} \log \frac{1}{\beta_{ij}} \\ &= \sum_{ij} \log \frac{2b}{b(a_{ij}^1 + a_{ij}^2) + (1-b)(2 - (a_{ij}^1 + a_{ij}^2))} \\ &= \sum_{ij} \log 2b - \sum_{ij} C_{ij}, \end{aligned}$$

where $C_{ij} = \log b(a_{ij}^1 + a_{ij}^2) + (1-b)(2 - (a_{ij}^1 + a_{ij}^2))$, and we have:

$$C_{ij} = \begin{cases} \log(b+1-b) = 0, & \text{if } a_{ij}^1 \neq a_{ij}^2, \\ \log 2b, & \text{if } a_{ij}^1 = a_{ij}^2 = 1, \\ \log 2(1-b), & \text{if } a_{ij}^1 = a_{ij}^2 = 0. \end{cases}$$

Let n , t and k be the numbers of all edges, $a_{ij}^1 = a_{ij}^2 = 1$ and $a_{ij}^1 = a_{ij}^2 = 0$ respectively, so we have:

$$H(\hat{\mathbf{S}}) \leq n \log 2b - t \log 2b - k \log 2(1-b).$$

Considering $d_{Ham} = \sum_{ij} |a_{ij}^1 - a_{ij}^2| = n - t - k$, we have:

$$H(\hat{\mathbf{S}}) \leq d_{Ham} \log 2b + k \log \frac{b}{1-b}.$$

So, the maximized $H(\hat{\mathbf{S}})$ is proportional to d_{Ham} , i.e., $H(\hat{\mathbf{S}}) \propto d_{Ham}$. \square

Using $H(\mathbf{A}^v, \hat{\mathbf{S}})$ (e.g., cross entropy) to depict the similarity between the distribution of $\hat{\mathbf{S}}$ and \mathbf{A}^v , and the belief $b^v \in (0, 1]$ can represent the relevance of v -th view to our clustering task, we have:

Theorem 2 (Task relevance of each graph). *For a specific graph, the more this graph relative to the clustering task, the more the distribution of $\hat{\mathbf{S}}$ similar to it, and vice versa:*

$$H(\mathbf{A}^v, \hat{\mathbf{S}}) \propto b^v. \quad (17)$$

Proof.

$$\begin{aligned} H(\mathbf{A}^v, \hat{\mathbf{S}}) &= \sum_{ij} a_{ij}^v \log \frac{1}{p(\hat{s}_{ij})} + (1 - a_{ij}^v) \log \frac{1}{1 - p(s_{ij})} \\ &= \sum_{i,j \in U} \log \frac{1}{\beta_{ij}} + \sum_{i,j \in T} \log \frac{1}{1 - \beta_{ij}}, \end{aligned}$$

where $U = \{i, j \mid a_{ij}^v = 1\}$ and $T = \{i, j \mid a_{ij}^v = 0\}$. Therefore, we have:

$$\begin{aligned} H(\mathbf{A}^v, \hat{\mathbf{S}}) &= \sum_{i,j \in U} \log \frac{\sum_{k=1}^V b^k}{b^v a_{ij}^v + (1-b^v)(1 - a_{ij}^v)} \\ &\quad + \sum_{i,j \in T} \log \frac{\sum_{k=1}^V b^k}{\sum_{k=1}^V b^k - b^v a_{ij}^v - (1-b^v)(1 - a_{ij}^v)} \\ &= \sum_{ij} \log \left(\sum_{k=1}^V b^k \right) - \left(\sum_{i,j \in U} \log b^v + \sum_{i,j \in T} \log (b^v - 1 + \sum_{k=1}^V b^k) \right) \\ &\Rightarrow H(\mathbf{A}^v, \hat{\mathbf{S}}) \propto b^v. \end{aligned}$$

From this equation, we can know that the more the v -th graph relative to the clustering task *i.e.*, b^v is larger, the more the $\hat{\mathbf{S}}$ is similar to this graph, *i.e.*, $H(\mathbf{A}^v, \hat{\mathbf{S}})$ is smaller. \square

From Theorem 1 and Theorem 2, we can conclude the following corollary:

Corollary 1. *The distribution of $\hat{\mathbf{S}}$ is dependent on the consistency of observed graphs and how much they are related to the clustering task.*

2) *Variational Graph Information Bottleneck:* To understand how the variational graph generator infers a graph with sufficient information, we build a connection between the objective function of the variational graph generator (Section III-C) and Information Bottleneck (IB) principle [44, 45]. Recall the definition of supervised IB [46]:

Definition 1 (Supervised IB). *The supervised IB is to maximize the Information Bottleneck Lagrangian:*

$$\mathcal{IB}_{sup} = I(Y, Z_X) - \omega I(X, Z_X), \text{ where } \omega > 0. \quad (18)$$

This shows that the supervised IB aims to maximize the mutual information between latent representation Z_X and corresponding target labels Y , meanwhile trying to compress more information from X (*i.e.*, minimize the mutual information between X and Z_X). The intuition behind IB is that the latent variable Z_X tries to collect less but sufficient information from X to facilitate the task.

Recall the proposed method, VGMGC aims at inferring the graph $\hat{\mathbf{S}}$ from global features $\bar{\mathbf{X}}$ in the inference process, and generating the observed graphs \mathbf{A}^v in the generative process. Intuitively, only the topological information in $\bar{\mathbf{X}}$ is useful and most others are redundant. Therefore, we can obtain our variational graph IB:

Definition 2 (Variational graph IB). *The IB in variational graph generator is:*

$$\mathcal{IB}_{graph} = \sum_v I(\mathbf{A}^v, \hat{\mathbf{S}}) - \omega I(\hat{\mathbf{S}}, \bar{\mathbf{X}}), \text{ where } \omega > 0. \quad (19)$$

Theorem 3. *Maximizing the ELBO (Eq. (7)) is equivalent to maximizing variational graph IB:*

$$\arg \max \mathcal{L}_E \cong \arg \max \mathcal{IB}_{graph}. \quad (20)$$

Proof. Here, \mathcal{IB}_{graph} is defined in Definition 2. For simplification, we rewrite mutual information as $I(\cdot; \cdot)$; \mathbf{A} , $\bar{\mathbf{X}}$, \mathbf{X}^v and $\hat{\mathbf{S}}$ as A , \bar{X} , X^v and \hat{S} .

Recall the property of mutual information:

$$\begin{aligned} I(X; Y | Z) &= I(X; Y) + H(Z | X) + H(Z | Y) \\ &\quad - H(Z | X, Y) - H(Z), \end{aligned}$$

where, $H(\cdot)$ denotes Entropy. From this property, we have:

$$\begin{aligned} I(A^v; \hat{S} | \bar{X}, X^v) &= I(A^v; \hat{S}) + H(\bar{X}, X^v | \hat{S}) \\ &\quad + H(\bar{X}, X^v | A^v) - H(\bar{X}, X^v | A^v, \hat{S}) - H(\bar{X}, X^v). \end{aligned}$$

Note that \bar{X} and X^v are observed, so $H(\bar{X})$ and $H(X^v)$ are two constants. We have:

$$I(A^v; \hat{S}) \propto I(A^v; \hat{S} | \bar{X}, X^v).$$

Let $p_D(a^v)$ denote data distribution of a^v , from the Bayesian network (Figure 2), we have the following derivation:

$$\begin{aligned} &I(A^v; \hat{S} | \bar{X}, X^v) \\ &= \mathbb{E}_{p(\bar{x}, x^v)} \int \int p(a^v, \hat{s} | \bar{x}, x^v) \log \frac{p(a^v, \hat{s} | \bar{x}, x^v)}{p_D(a^v | \bar{x}, x^v) q(\hat{s} | \bar{x}, x^v)} d\hat{s} da^v \\ &= \mathbb{E}_{p(\bar{x}) p(x^v)} \int \int p_D(a^v) q(\hat{s} | \bar{x}) \log \frac{p(a^v | \hat{s}, x^v)}{p_D(a^v)} d\hat{s} da^v \\ &= \mathbb{E}_{p(\bar{x}) p(x^v)} \int \int p_D(a^v) q(\hat{s} | \bar{x}) \log p(a^v | \hat{s}, x^v) d\hat{s} da^v \\ &\quad + H(A^v) \\ &\geq \mathbb{E}_{p(\bar{x}) p(x^v)} \int \int p_D(a^v) q(\hat{s} | \bar{x}) \log p(a^v | \hat{s}, x^v) d\hat{s} da^v \\ &\geq \mathbb{E}_{p(\bar{x}) p(x^v)} \mathbb{E}_{q(\hat{s} | \bar{x})} \log p_{\xi^v}(a^v | \hat{s}, x^v), \end{aligned} \quad (21)$$

where $p_{\xi^v}(a^v | \hat{s}, x^v)$ is a variational approximation of $p(a^v | \hat{s}, x^v)$. The last term of Eq. (21) is deduced from $KL(p(a^v | \hat{s}, x^v) || p_{\xi^v}(a^v | \hat{s}, x^v)) \geq 0$. Therefore, we have obtained the first term in \mathcal{L}_E from Eq. (21). For the second term, we have:

$$\begin{aligned} I(\hat{S}, \bar{X}) &= \int \int q(\hat{s}, \bar{x}) \log \frac{q(\hat{s}, \bar{x})}{q(\hat{s}) p(\bar{x})} d\bar{x} d\hat{s} \\ &= \mathbb{E}_{p(\bar{x})} \int q(\hat{s} | \bar{x}) \log \frac{q(\hat{s} | \bar{x}) p(\hat{s})}{q(\hat{s}) p(\hat{s})} d\hat{s} \\ &\leq \mathbb{E}_{p(\bar{x})} KL(q(\hat{s} | \bar{x}) || p(\hat{s})). \end{aligned} \quad (22)$$

Here, $p(\hat{s})$ and $p(\bar{x})$ denote the prior distribution of \hat{s} and data distribution of \bar{x} , and $q(\cdot)$ denotes the distribution can be approximated. This upper bound is the second term in \mathcal{L}_E . So, Theorem 3 can be obtained by concluding the above formulas:

$$\begin{aligned} \arg \max I(A^v, \hat{S}) - \omega I(\hat{S}, \bar{X}) &\cong \arg \max \mathbb{E}_{q(\hat{s} | \bar{x})} \log p_{\xi^v}(a^v | \hat{s}, x^v) \\ &\quad - \omega KL(q(\hat{s} | \bar{x}) || p(\hat{s})) \\ &\Rightarrow \arg \max \mathcal{IB}_{graph} \cong \arg \max \mathcal{L}_E. \end{aligned}$$

\square

Eq. (20) indicates that by optimizing Eq. (7), the consensus graph $\hat{\mathbf{S}}$ can capture the most useful topological information and discard redundant information from global feature $\bar{\mathbf{X}}$.

3) *Lower Bound of Mutual Information:* Following [47, 48], we analyze the lower bound of mutual information for optimizing $I(\mathbf{Z}^v, \mathbf{X}^v)$ and $I(\alpha^v, \bar{\mathbf{X}})$.

Definition 3. *The mutual information $I(\mathbf{Z}^v, \mathbf{X}^v)$ is:*

$$I(\mathbf{Z}^v, \mathbf{X}^v) = \mathbb{E}_{p(\mathbf{z}^v, \mathbf{x}^v)} \log \frac{p(\mathbf{z}^v, \mathbf{x}^v)}{p(\mathbf{z}^v) p(\mathbf{x}^v)}. \quad (23)$$

Considering that the entropy $H(\cdot)$ is always positive, we have:

$$\begin{aligned} &I(\mathbf{Z}^v, \mathbf{X}^v) \\ &= \int \int p(\mathbf{z}^v, \mathbf{x}^v) \log \frac{p(\mathbf{x}^v | \mathbf{z}^v)}{p(\mathbf{x}^v)} d\mathbf{x}^v d\mathbf{z}^v \\ &= \int \int p(\mathbf{x}^v) p(\mathbf{z}^v | \mathbf{x}^v) \log p(\mathbf{x}^v | \mathbf{z}^v) d\mathbf{x}^v d\mathbf{z}^v \\ &\quad + \int \int p(\mathbf{x}^v) p(\mathbf{z}^v | \mathbf{x}^v) \log \frac{1}{p(\mathbf{x}^v)} d\mathbf{x}^v d\mathbf{z}^v \\ &= \int \int p(\mathbf{x}^v) p(\mathbf{z}^v | \mathbf{x}^v) \log p(\mathbf{x}^v | \mathbf{z}^v) d\mathbf{x}^v d\mathbf{z}^v + H(\mathbf{x}^v) \\ &\geq \int \int p(\mathbf{x}^v) p(\mathbf{z}^v | \mathbf{x}^v) \log p(\mathbf{x}^v | \mathbf{z}^v) d\mathbf{x}^v d\mathbf{z}^v. \end{aligned}$$

TABLE I
THE STATISTICS INFORMATION OF EXPERIMENTAL DATASETS.

Dataset	#Clusters	#Nodes	#Features	Graphs
ACM	3	3025	1830	\mathcal{G}^1 co-paper \mathcal{G}^2 co-subject
DBLP	4	4057	334	\mathcal{G}^1 co-author \mathcal{G}^2 co-conference \mathcal{G}^3 co-term
Photos	8	7487	$\frac{745}{7487}$	\mathcal{G}^1 co-purchase
Computers	10	13381	$\frac{767}{13381}$	\mathcal{G}^1 co-purchase
Cora	7	2708	1433	\mathcal{G}^1 citation network
Citeseer	6	3327	3703	\mathcal{G}^1 citation network
BBC Sport	5	544	$\frac{3283}{3183}$	\mathcal{G}^1 kNN graph \mathcal{G}^2 kNN graph
3Sources	6	169	$\frac{3560}{3631}$ $\frac{3068}{3631}$	\mathcal{G}^1 kNN graph \mathcal{G}^2 kNN graph \mathcal{G}^3 kNN graph

Here, because $p(\mathbf{x}^v | \mathbf{z}^v)$ is intractable, $q_{\eta^v}(\mathbf{x}^v | \mathbf{z}^v)$ is introduced as a variational approximation of $p(\mathbf{x}^v | \mathbf{z}^v)$. Considering that KL divergence is always positive, i.e., $KL(p(\mathbf{x}^v | \mathbf{z}^v) || q_{\eta^v}(\mathbf{x}^v | \mathbf{z}^v)) \geq 0$, we can obtain the lower bound of mutual information:

$$\begin{aligned}
& \int \int p(\mathbf{x}^v) p(\mathbf{z}^v | \mathbf{x}^v) \log p(\mathbf{x}^v | \mathbf{z}^v) d\mathbf{x}^v d\mathbf{z}^v \\
&= \int \int p(\mathbf{x}^v) p(\mathbf{z}^v | \mathbf{x}^v) \log \frac{p(\mathbf{x}^v | \mathbf{z}^v)}{q_{\eta^v}(\mathbf{x}^v | \mathbf{z}^v)} q_{\eta^v}(\mathbf{x}^v | \mathbf{z}^v) d\mathbf{x}^v d\mathbf{z}^v \\
&= \int \int p(\mathbf{z}^v) KL(p(\mathbf{x}^v | \mathbf{z}^v) || q_{\eta^v}(\mathbf{x}^v | \mathbf{z}^v)) d\mathbf{x}^v d\mathbf{z}^v \\
&\quad + \int \int p(\mathbf{x}^v) p(\mathbf{z}^v | \mathbf{x}^v) \log q_{\eta^v}(\mathbf{x}^v | \mathbf{z}^v) d\mathbf{x}^v d\mathbf{z}^v \\
&\geq \int \int p(\mathbf{x}^v) p(\mathbf{z}^v | \mathbf{x}^v) \log q_{\eta^v}(\mathbf{x}^v | \mathbf{z}^v) d\mathbf{x}^v d\mathbf{z}^v \\
&= \mathbb{E}_{p(\mathbf{x}^v) p(\mathbf{z}^v | \mathbf{x}^v)} \log q_{\eta^v}(\mathbf{x}^v | \mathbf{z}^v).
\end{aligned}$$

Therefore, the mutual information here can be maximized by maximizing its lower bound:

$$\arg \max I(\mathbf{Z}^v, \mathbf{X}^v) \cong \arg \max \mathbb{E}_{p(\mathbf{x}^v) p(\mathbf{z}^v | \mathbf{x}^v)} \log q_{\eta^v}(\mathbf{x}^v | \mathbf{z}^v). \quad (24)$$

In our case, x_j^v is subordinated to Bernoulli distribution, so $-\mathbb{E}_{p(\mathbf{z}^v | \mathbf{x}^v) p(\mathbf{x}^v)} \log q_{\eta^v}(\mathbf{x}^v | \mathbf{z}^v)$ can be instantiated by a binary cross entropy loss between \mathbf{x}^v and its reconstruction $\tilde{\mathbf{x}}^v$. The lower bound of all $I(\mathbf{Z}^v, \mathbf{X}^v)$ and $I(\alpha, \bar{\mathbf{X}})$ are added together, written as \mathcal{L}_r .

IV. EXPERIMENTS

A. Experimental Settings

1) *Datasets*: Four common benchmark multi-view graph datasets, i.e., ACM, DBLP, Amazon photos, and Amazon computers, two traditional single-view graph datasets Cora and Citeseer, and two traditional multi-view datasets BBC Sport and 3Sources, are selected to evaluate the proposed VGMGC.

The statistics information of these datasets are listed in Table I. Specifically,

- **ACM¹**: This is a paper network from the ACM database. It consists of two different graphs, co-paper and co subject, represents the relationship of the same author with papers and the relationship of the same subject with papers respectively. The node feature is a bag-of-words representation of each paper's keywords.
- **DBLP²**: This is an author network from the DBLP database. The dataset includes three graphs, i.e. co-author (co-authors for the same paper), co-conference (papers published on the same conference) and co-term (papers published on the same term). The node feature is a bag-of-words representation of each author's keywords.
- **Amazon datasets**: Amazon photos and Amazon computers are the subsets of the Amazon co-purchase network from [19]. The network means the two goods that are purchased together. The node feature is a bag-of-words representation of each good's product reviews. Due to Amazon photos and Amazon computers only having single-view features, we constructed the second view features through cartesian product following by [6].
- **Cora³ and Citeseer⁴**: Cora and Citeseer are two classical single-view graph datasets. Each node represent a paper with features extracted from bag-of-word of the paper. The network is a paper citation network.
- **BBC Sport⁵**: BBC Sport is a widely-used traditional multi-view dataset. Each node is a document from one of five classes with two features extracted from the document. Two graphs are constructed from features in SDSNE [28].
- **3Sources⁶**: 3Sources is a traditional multi-view dataset, containing 169 reports reported in different three sources. Each node represents a reports with three features extracted from three sources respectively. The graphs are constructed from features in SDSNE [28].

2) *Comparison Methods*: On four multi-view graph datasets, our comparison methods in Table II can be divided into three categories:

- **Single-view baselines**: LINE & GAE: LINE [49] and GAE [32] are two typical single-view clustering methods.
- **Multi-view graph baselines**: PMNE [50], SwMC [51] and MNE [52] are four classical multi-view clustering methods which try to generate final embedding for clustering. RMSC [12] is a robust spectral clustering model.
- **SOTAs**: O2MAC [7] and MAGCN [6] are the methods that learn from both attribute features and structural information. In addition, graph filter-based MGC methods, like MvAGC [20] and MCGC [19], are included. COMPLETER [53] and MVGRL [54] are contrastive learning methods to learn a common representation for clustering.

¹<https://dl.acm.org/>

²<https://dblp.uni-trier.de/>

³<https://graphsandnetworks.com/the-cora-dataset/>

⁴<https://deeppai.org/dataset/citeseer>

⁵<http://mlg.ucd.ie/datasets/bbc.html>

⁶<http://mlg.ucd.ie/datasets/3sources.html>

TABLE II

THE OVERALL CLUSTERING RESULTS. THE VALUES IN THE TABLE ARE SHOWN AS PERCENTAGE. THE BEST RESULTS ARE SHOWN IN BOLD, AND ‘—’ DENOTES THE RESULTS NOT REPORTED IN THE ORIGINAL PAPERS.

Methods / Datasets	Amazon photos				Amazon computers			
	NMI	ARI	ACC	F1	NMI	ARI	ACC	F1
MAGCN [6] (2020)	39.0	24.0	51.7	47.3	—	—	—	—
COMPLETER [53] (2021)	26.1	7.6	36.8	30.7	15.6	5.4	24.2	16.0
MVGRL [54] (2021)	43.3	23.8	50.5	46.0	10.1	5.5	24.5	17.1
MvAGC [20] (2021)	52.4	39.7	67.8	64.0	39.6	32.2	58.0	41.2
MCGC [19] (2021)	61.5	43.2	71.6	68.6	53.2	39.0	59.7	52.0
VGMGC (ours)	66.8	58.4	78.5	76.9	53.5	47.5	62.2	50.2
Methods / Datasets	ACM				DBLP			
RMSC [12] (2014)	39.7	33.1	63.2	57.5	71.1	76.5	89.9	82.5
LINE [49] (2015)	39.4	34.3	64.8	65.9	66.8	69.9	86.9	85.5
GAE [32] (2016)	49.1	54.4	82.2	82.3	69.3	74.1	88.6	87.4
PMNE [50] (2017)	46.5	43.0	69.4	69.6	59.1	52.7	79.3	79.7
SwMC [51] (2017)	8.4	4.0	41.6	47.1	37.6	38.0	65.4	56.0
MNE [52] (2018)	30.0	24.9	63.7	64.8	—	—	—	—
O2MAC [7] (2020)	69.2	73.9	90.4	90.5	72.9	77.8	90.7	90.1
MvAGC [20] (2021)	67.4	72.1	89.8	89.9	77.2	82.8	92.8	92.3
MCGC [19] (2021)	71.3	76.3	91.5	91.6	83.0	77.5	93.0	92.5
VGMGC (ours)	76.3	81.9	93.6	93.6	78.3	83.7	93.2	92.7

On other traditional two single-graph and two multi-view datasets, six baselines dedicated to single-graph clustering and four baselines dedicated to multi-view clustering are chosen. Specifically:

- Traditional single-graph clustering methods: VGAE [32], ARVGE [33], and GMM-VGAE [55] are three variational-based methods; DAEGC [56] and MAGCN [6] are two SOTAs conducted on single-view graph data.
- Traditional multi-view clustering methods: GMC [13], CGD [57] and SDSNE [28] are three graph-based multi-view clustering SOTAs. They learn a unified graph from multi-view data for multi-view clustering; O2MAC [7] conducts GNN for multi-view clustering.

3) *Evaluations*: Following the work of the pioneers, we adopt four common metrics, *i.e.* normalized mutual information (NMI), adjusted rand index (ARI), accuracy (ACC) and F1-score (F1), as the metrics to evaluate the clustering performance of the proposed VGMGC. For comparison, we collect the best reported performances from the literature. More implementation details can be found in Appendix B.

B. Overall Results

Table II shows the clustering performance of the proposed VGMGC and comparison methods on four multi-graph datasets. Intuitively, VGMGC outperforms the best SOTA, *i.e.* MCGC, with ACC boosting 6.9%, 2.5%, 2.1% and 0.1% on the four different datasets respectively. Moreover, it shows an overwhelming advantage with respect to ACM and Amazon photos, improving NMI both by more than 5%. In all, with the help of the generated variational consensus graph, the proposed VGMGC achieves superior performance compared with the existing MGC SOTAs.

TABLE III

CLUSTERING RESULTS ON TWO SINGLE-VIEW GRAPH DATASETS (CORa AND CITeseer) AND TWO TRADITIONAL MULTI-VIEW DATASETS (BBC SPORT AND 3Sources). THE VALUES IN THE TABLE ARE SHOWN AS PERCENTAGE. THE BEST RESULTS ARE SHOWN IN BOLD, AND ‘—’ REPRESENTS THE RESULTS NOT REPORTED IN THE ORIGINAL PAPERS.

Methods / Datasets	Cora				Citeseer			
	NMI	ARI	ACC	F1	NMI	ARI	ACC	F1
VGAE [32] (2016)	40.8	34.7	59.2	45.6	16.3	10.1	39.2	27.8
ARVGE [33] (2018)	45.0	37.4	63.8	62.7	26.1	24.5	54.4	52.9
AGC [1] (2019)	53.7	44.8	68.9	65.6	41.1	42.0	67.0	62.3
DAEGC [56] (2019)	52.8	49.6	70.4	68.2	39.7	41.0	67.2	63.6
GMM-VGAE [55] (2020)	54.4	—	71.5	67.8	42.3	—	67.4	63.2
MAGCN [6] (2020)	55.3	47.6	71.0	—	41.8	40.3	69.8	—
VGMGC (ours)	57.2	53.5	73.6	71.6	44.7	46.5	69.9	65.2
Methods / Datasets	BBC Sport				3Sources			
GMC [13] (2020)	70.5	60.1	73.9	72.1	54.8	44.3	69.2	60.5
CGD [57] (2020)	91.0	93.1	97.4	94.7	69.5	61.1	78.1	70.9
O2MAC [7] (2020)	89.1	90.6	96.4	96.5	72.7	75.5	65.0	66.9
SDSNE [28] (2022)	94.8	95.8	98.5	96.8	84.8	86.7	93.5	89.8
VGMGC (ours)	96.1	96.9	98.9	99.0	85.9	87.6	94.1	92.7

C. Generalization to Other Datasets

In this section, we explore how well VGMGC performed on other two types of datasets, *i.e.*, single-view graph datasets Cora and Citeseer, and traditional multi-view datasets 3Sources and BBC Sport.

In Table III it is clear that VGMGC performs best on both single-view graph datasets and traditional multi-view datasets compared with previous SOTAs. Specifically, we can see that the F1 score of VGMGC increases 3.4% on Cora and 2.9% on 3Sources compared to the previous SOTAs, DAEGC and SDSNE, respectively, which demonstrates that VGMGC can be well generalized to both single-view graph clustering and traditional multi-view clustering tasks.

D. Ablation Study

We present the ablation study of VGMGC on ACM and DBLP datasets in this subsection, including the effect of each component and the performance on each single view.

1) *Effect of Each Component*: As shown in the upper part of Table IV, without any of the components, the performance of VGMGC is negatively affected to varying degrees. Specifically, the generated consensus graph \hat{S} plays an important role. Without the consensus graph and its guidance (see w/o \hat{S} & \mathcal{L}_E), the dramatic drop in performance demonstrates that the variational consensus graph \hat{S} can mine enough global topological information. \mathcal{L}_r also makes a considerable contribution to the overall performance (see w/o \mathcal{L}_r), as the Z^v of specific view can preserve useful information from X^v . Furthermore, this means the latent representations \bar{Z} has included enough clustering information. Thus, the clustering loss \mathcal{L}_c is helpful, while it seems to be faint (see w/o \mathcal{L}_c).

2) *Performance on Each View*: We run VGMGC on each single view to test how much effect VGMGC has gained from these multiple views helping with each other. The last three rows of Table IV show the results (see VGMGC-single), and Figure 3 depicts the task relevance of each view

TABLE IV

THE ABLATION STUDY RESULTS ON ACM AND DBLP. THE ORIGINAL RESULTS OF VGMGC ARE SHOWN IN BOLD, AND THE THIRD VIEW \mathcal{G}^3 THAT DOES NOT EXIST IN ACM IS DENOTED BY '*'. VALUES IN PARENTHESES COMPARE THE PERFORMANCE WITH THE ORIGINAL VGMGC.

Components	ACM				DBLP			
	NMI%	ARI%	ACC%	F1%	NMI%	ARI%	ACC%	F1%
w/o \mathcal{L}_c	75.0 (-1.3)	80.6 (-1.3)	93.1 (-0.5)	93.1 (-0.5)	77.9 (-0.4)	83.2 (-0.5)	93.0 (-0.2)	92.4 (-0.3)
w/o \mathcal{L}_r	67.6 (-8.7)	70.4 (-11.5)	88.7 (-4.9)	88.4 (-5.2)	76.2 (-2.1)	81.4 (-2.3)	92.1 (-1.1)	91.3 (-1.4)
w/o $\hat{\mathcal{S}}$ & \mathcal{L}_E	44.4 (-31.9)	42.4 (-39.5)	70.9 (-22.7)	71.4 (-22.2)	20.7 (-57.6)	17.8 (-65.9)	47.1 (-46.1)	44.8 (-47.9)
VGMGC-single (\mathcal{G}^1)	73.1(-3.2)	79.6(-1.3)	92.8(-0.8)	92.8(-0.8)	47.7(-30.6)	52.5(-31.2)	79.0(-14.2)	78.6(-14.1)
VGMGC-single (\mathcal{G}^2)	59.3(-17.0)	61.2(-20.7)	84.4(-9.2)	84.0(-9.6)	75.8(-2.5)	80.9(-2.8)	91.9(-1.3)	91.0(-1.7)
VGMGC-single (\mathcal{G}^3)	*	*	*	*	15.6(-62.7)	11.1(-72.6)	45.9(-47.3)	45.3(-47.4)
Original	76.3	81.9	93.6	93.6	78.3	83.7	93.2	92.7

TABLE V

EXPERIMENTS OF LARGER τ ON ACM. THE LAST TWO COLUMNS DENOTES THE MEAN AND VARIANCE OF s_{ij} COMPUTED FROM TRAINING VGMGC WITH 200 EPOCHS.

Temperature	NMI%	ACC%	Mean (1e-2)	Variance (1e-2)
$\tau = 0.1$	77.4	93.8	50.46	22.5
$\tau = 1$	77.5	93.9	50.297	8.337
$\tau = 2$	77.7	94.0	50.192	3.542
$\tau = 5$	77.7	94.1	50.091	0.758
$\tau = 10$	77.7	94.0	50.046	0.201
$\tau = 50$	77.6	94.0	50.009	8.217 (1e-5)
$\tau = 100$	77.2	93.9	50.0004	2.056 (1e-5)

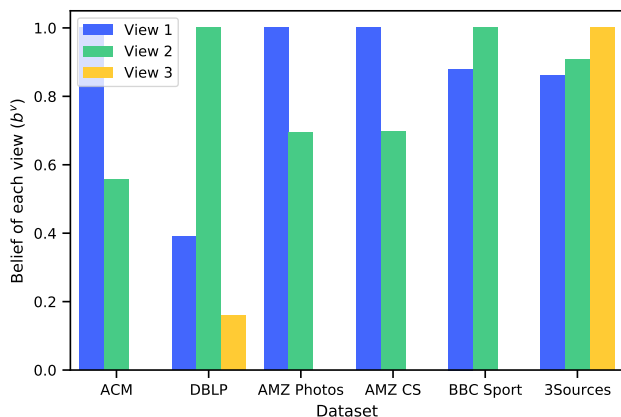


Fig. 3. The learned b^v on six multi-view datasets, which shows the task relevance of each view. The parameter ρ is fixed to 1 in this figure. ‘AMZ’ means Amazon and ‘CS’ denotes Computers.

(b^v) learned by VGMGC on six multi-view datasets. From Table IV, we can see that the clustering results of VGMGC (original) outperforms all other single views, which indicates that VGMGC can take advantage of all views to obtain better clustering results. For example, on DBLP, even though the first graph and third graph perform badly as View 1 and View 3 shown in Figure 3, the NMI of VGMGC still increases by 2.5% comparing to the best single-view results (VGMGC-single (\mathcal{G}^2)). We also visualize the clustering results of each view on DBLP in Section IV-E4.

E. Analysis and Visualization

1) *Oversmoothing Analysis*: The left side of Figure 4 shows the performance with different orders. Overall, the

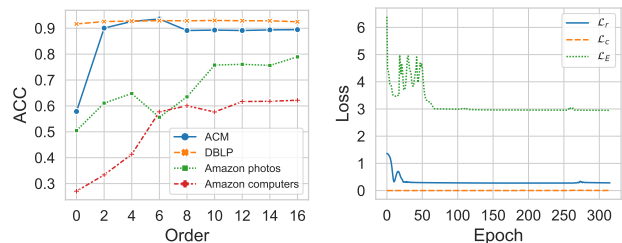


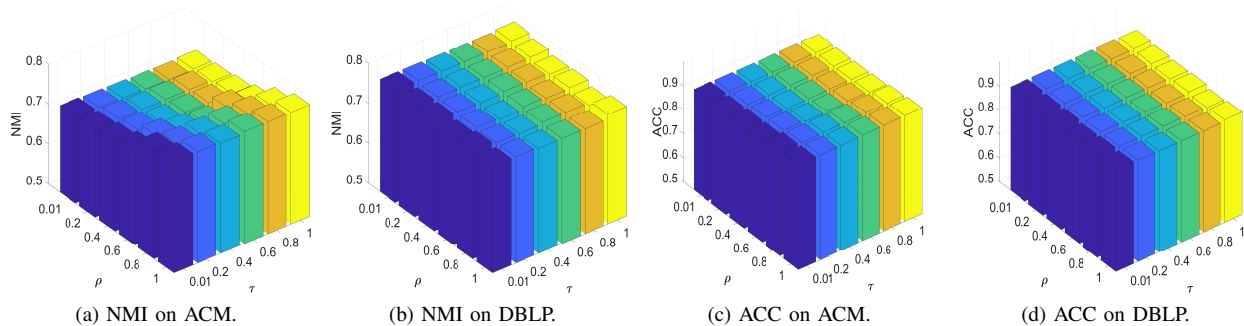
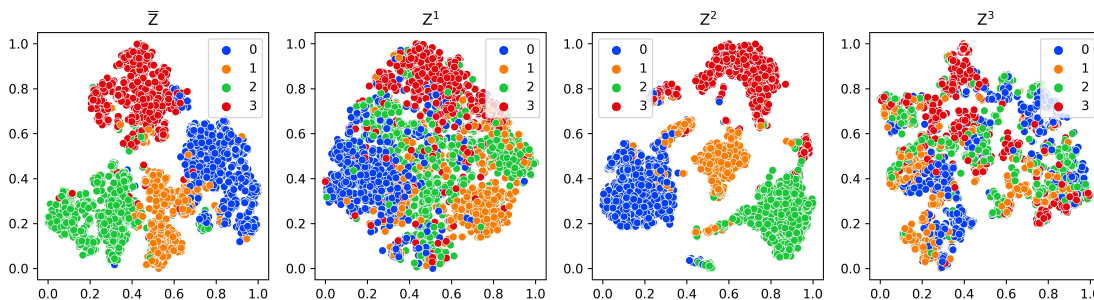
Fig. 4. Left depicts the performance with different orders. Right depicts the training process on ACM.

ACC increases with the increase of order, which suggests that VGMGC can mitigate oversmoothing. Notably, the plot on DBLP is steady, a possible explanation for this might be that VGMGC has learnt sufficient clustering-related information from original features directly.

2) *Convergence Analysis*: The right side of Figure 4 shows the trend of losses with training epochs. We can see that all losses converge after training around 100 epochs. Specifically, the value of \mathcal{L}_E is large and \mathcal{L}_c is relatively small.

3) *Parameter Sensitive Analysis*: Figure 5 depicts how much the parameter ρ and τ influence VGMGC. In general, the influences of both ρ and τ are minor to VGMGC, and ρ is more influential than τ . We also can see that the ACC performs stable on the two datasets with the variation of ACC within 3%. Looking into the results of NMI, VGMGC has a more stable performance on DBLP. Specifically, it can be seen that NMI trends to increase on ACM but decrease on DBLP as the hyper-parameter ρ increases. We could speculate that the information from different views may be harmful on ACM but more compatible and helpful on DBLP. This is due to the fact that the ρ determines how much the bad view influence our model, as discussed in Section III-E. VGMGC, on the other hand, behaves relatively stable for different values of τ which impacts on the distribution of s_{ij} .

Furthermore, we explore a wider range of τ to see how it influences the distribution of generated graph. The distribution of generated graph is represented by the mean and variance of s_{ij} . From Table V, the variance of s_{ij} falls and its mean value closes to 50% gradually as τ increasing. This is because increasing τ injects more noise whose distribution subjects to $Uniform(0, 1)$ to s_{ij} , which is consistent with the theory.

Fig. 5. Sensitive analysis with ρ and τ on ACM and DBLP.Fig. 6. The visualization of t -SNE on each view's latent representation of DBLP dataset. \bar{Z} denotes the multi-view fused latent representation, and the rest denote other views' representation of the dataset.

4) *Visualization of Each View*: In order to obtain a more intuitive understanding of the clustering performance of the proposed VGMGC, each view's embedding is visualized in Figure 6. We can see that the third view Z^3 in DBLP performs poorly, while Z^2 in DBLP performs relatively well. It is notably that the generated variational fused view \bar{Z} can differentiate some ambiguous points in the second view Z^2 . This fused view manages to have an impressive performance because it can mine enough view-specific and view-common information from each specific view. This corroborates the results in Section IV-D2.

V. CONCLUSIONS

In this paper, we proposed a multi-view graph clustering method to better mine and embed the consensus topological information of all graphs while reserving useful feature information and extracting some task relevant information, which is called variational graph generator for multi-view graph clustering (VGMGC). We also theoretically proved its effectiveness from information theories. Our experiments showed that VGMGC outperforms previous MGC works on eight datasets. In the future, we expect our work could inspire more researches, such as graph generation and multi-graph learning. A limitation of the proposed method is that it limited to the clustering task. For other tasks, it needs to change the score function to compute the belief of each graph.

ACKNOWLEDGEMENTS

This work was supported in part by Sichuan Science and Technology Program (Nos. 2021YFS0172, 2022YFS0047, and

2022YFS0055), Medico-Engineering Cooperation Funds from University of Electronic Science and Technology of China (No. ZYGX2021YGLH022), the National Science Foundation (MRI 2215789), and Lehigh's grants (S00010293 and 001250).

REFERENCES

- [1] X. Zhang, H. Liu, Q. Li, and X.-M. Wu, "Attributed graph clustering via adaptive graph convolution," in *IJCAI*, 2019, pp. 4327–4333.
- [2] P. Velickovic, W. Fedus, W. L. Hamilton, P. Liò, Y. Bengio, and R. D. Hjelm, "Deep graph infomax," *ICLR*, 2019.
- [3] F. Wu, A. H. S. Jr., T. Zhang, C. Fifty, T. Yu, and K. Q. Weinberger, "Simplifying graph convolutional networks," in *ICML*, 2019, pp. 6861–6871.
- [4] Z. A. Kakarash, N. F. Ahmed, and K. M. Hamakarim, "A temporal and social network-based recommender using graph clustering," *Passer Journal of Basic and Applied Sciences*, 2022.
- [5] D. Jin, Z. Yu, P. Jiao, S. Pan, D. He, J. Wu, P. Yu, and W. Zhang, "A survey of community detection approaches: From statistical modeling to deep learning," *TKDE*, pp. 1–1, 2021.
- [6] J. Cheng, Q. Wang, Z. Tao, and Q. Gao, "Multi-view attribute graph convolution networks for clustering," in *IJCAI*, 2020, pp. 2973–2979.
- [7] S. Fan, X. Wang, C. Shi, E. Lu, K. Lin, and B. Wang, "One2multi graph autoencoder for multi-view graph clustering," in *WWW*, 2020, pp. 3070–3076.
- [8] Y. Liang, D. Huang, C.-D. Wang, and P. S. Yu, "Multi-view graph learning by joint modeling of consistency and inconsistency," *TNNLS*, pp. 1–15, 2022.
- [9] F. Nie, J. Li, and X. Li, "Self-weighted multiview clustering with multiple graphs," in *IJCAI*, 2017, pp. 2564–2570.
- [10] S. Shi, F. Nie, R. Wang, and X. Li, "Multi-view clustering via nonnegative and orthogonal graph reconstruction," *TNNLS*, pp. 1–14, 2021.

- [11] X. Yang, C. Deng, Z. Dang, and D. Tao, "Deep multiview collaborative clustering," *TNNLS*, pp. 1–11, 2021.
- [12] R. Xia, Y. Pan, L. Du, and J. Yin, "Robust multi-view spectral clustering via low-rank and sparse decomposition," in *AAAI*, 2014, p. 2149–2155.
- [13] H. Wang, Y. Yang, and B. Liu, "Gmc: Graph-based multi-view clustering," *TKDE*, vol. 32, no. 6, pp. 1116–1129, 2020.
- [14] X. L. Li, M. S. Chen, C. D. Wang, and J. H. Lai, "Refining graph structure for incomplete multi-view clustering," *TNNLS*, pp. 1–14, 2022.
- [15] J. Macqueen, "Some methods for classification and analysis of multivariate observations," in *In 5-th Berkeley Symposium on Mathematical Statistics and Probability*, 1967, pp. 281–297.
- [16] T. N. Kipf and M. Welling, "Semi-supervised classification with graph convolutional networks," in *ICLR*, 2017.
- [17] P. Veličković, G. Cucurull, A. Casanova, A. Romero, P. Liò, and Y. Bengio, "Graph attention networks," in *ICLR*, 2018.
- [18] H. Zhu and P. Koniusz, "Simple spectral graph convolution," in *ICLR*, 2021.
- [19] E. Pan and Z. Kang, "Multi-view contrastive graph clustering," *NeurIPS*, vol. 34, pp. 2148–2159, 2021.
- [20] Z. Lin and Z. Kang, "Graph filter-based multi-view attributed graph clustering," in *IJCAI*, 2021, pp. 19–26.
- [21] C. Zheng, B. Zong, W. Cheng, D. Song, J. Ni, W. Yu, H. Chen, and W. Wang, "Robust graph representation learning via neural sparsification," in *ICML*, 2020, pp. 11 458–11 468.
- [22] C. Morris and P. Mutzel, "Towards a practical k-dimensional weisfeiler-leman algorithm," in *NeurIPS*, 2020.
- [23] K. Xu, W. Hu, J. Leskovec, and S. Jegelka, "How powerful are graph neural networks?" in *ICLR*, 2019.
- [24] Y. Ren, J. Pu, Z. Yang, J. Xu, G. Li, X. Pu, P. S. Yu, and L. He, "Deep clustering: A comprehensive survey," *ArXiv*, vol. abs/2210.04142, 2022.
- [25] Z. Huang, Y. Ren, X. Pu, L. Pan, D. Yao, and G. Yu, "Dual self-paced multi-view clustering," *Neural Networks*, vol. 140, pp. 184–192, 2021.
- [26] J. Xu, Y. Ren, H. Tang, Z. Yang, L. Pan, Y. Yang, and X. Pu, "Self-supervised discriminative feature learning for deep multi-view clustering," *TKDE*, 2022.
- [27] J. Xie, R. Girshick, and A. Farhadi, "Unsupervised deep embedding for clustering analysis," in *ICML*, 2016, pp. 478–487.
- [28] C. Liu, Z. Liao, Y. Ma, and K. Zhan, "Stationary diffusion state neural estimation for multiview clustering," in *AAAI*, 2022, pp. 7542–7549.
- [29] D. P. Kingma and M. Welling, "Auto-encoding variational bayes," in *ICLR*, 2014.
- [30] N. Dilokthanakul, P. A. Mediano, M. Garnelo, M. C. Lee, H. Salimbeni, K. Arulkumaran, and M. Shanahan, "Deep unsupervised clustering with gaussian mixture variational autoencoders," *arXiv preprint arXiv:1611.02648*, 2016.
- [31] J. Xu, Y. Ren, H. Tang, X. Pu, X. Zhu, M. Zeng, and L. He, "Multi-VAE: Learning disentangled view-common and view-peculiar visual representations for multi-view clustering," in *ICCV*, 2021, pp. 9214–9223.
- [32] T. N. Kipf and M. Welling, "Variational graph auto-encoders," in *NeurIPS*, 2016.
- [33] S. Pan, R. Hu, G. Long, J. Jiang, L. Yao, and C. Zhang, "Adversarially regularized graph autoencoder for graph embedding," in *IJCAI*, 2018, pp. 2609–2615.
- [34] L. Sun, Z. Zhang, J. Zhang, F. Wang, H. Peng, S. Su, and P. S. Yu, "Hyperbolic variational graph neural network for modeling dynamic graphs," in *AAAI*, 2021.
- [35] D. Luo, W. Cheng, D. Xu, W. Yu, B. Zong, H. Chen, and X. Zhang, "Parameterized explainer for graph neural network," in *NeurIPS*, 2020.
- [36] P. Elinas, E. V. Bonilla, and L. C. Tiao, "Variational inference for graph convolutional networks in the absence of graph data and adversarial settings," in *NeurIPS*, 2020.
- [37] E. N. Gilbert, "Random Graphs," *Ann Stat*, vol. 30, no. 4, pp. 1141 – 1144, 1959.
- [38] A. Vaswani, N. Shazeer, N. Parmar, J. Uszkoreit, L. Jones, A. N. Gomez, L. Kaiser, and I. Polosukhin, "Attention is all you need," in *NeurIPS*, 2017, p. 6000–6010.
- [39] E. Jang, S. Gu, and B. Poole, "Categorical reparameterization with gumbel-softmax," *arXiv preprint arXiv:1611.01144*, 2016.
- [40] C. J. Maddison, A. Mnih, and Y. W. Teh, "The concrete distribution: A continuous relaxation of discrete random variables," *arXiv preprint arXiv:1611.00712*, 2016.
- [41] M. Chen, Z. Wei, Z. Huang, B. Ding, and Y. Li, "Simple and deep graph convolutional networks," in *ICML*, 2020, pp. 1725–1735.
- [42] J. Xu, Y. Ren, G. Li, L. Pan, C. Zhu, and Z. Xu, "Deep embedded multi-view clustering with collaborative training," *Inf. Sci.*, vol. 573, pp. 279–290, 2021.
- [43] L. v. d. Maaten and G. Hinton, "Visualizing data using t-sne," *JMLR*, vol. 9, no. 2605, pp. 2579–2605, 2008.
- [44] A. A. Alemi, I. Fischer, J. V. Dillon, and K. Murphy, "Deep variational information bottleneck," in *ICLR*, 2017.
- [45] R. A. Amjad and B. C. Geiger, "Learning representations for neural network-based classification using the information bottleneck principle," *TPAMI*, vol. 42, no. 9, pp. 2225–2239, 2020.
- [46] N. Tishby, F. C. Pereira, and W. Bialek, "The information bottleneck method," *arXiv preprint physics/0004057*, 2000.
- [47] I. Belghazi, S. Rajeswar, A. Baratin, R. D. Hjelm, and A. C. Courville, "Mutual information neural estimation," in *ICML*, 2018.
- [48] B. Poole, S. Ozair, A. van den Oord, A. A. Alemi, and G. Tucker, "On variational bounds of mutual information," in *ICML*, 2019.
- [49] J. Tang, M. Qu, M. Wang, M. Zhang, J. Yan, and Q. Mei, "Line: Large-scale information network embedding," in *WWW*, 2015, pp. 1067–1077.
- [50] W. Liu, P.-y. Chen, S. Yeung, T. Suzumura, and L. Chen, "Principled multilayer network embedding," in *ICDMW*, 2017, pp. 134–141.
- [51] F. Nie, J. Li, X. Li *et al.*, "Self-weighted multiview clustering with multiple graphs," in *IJCAI*, 2017, pp. 2564–2570.
- [52] K. Zhan, F. Nie, J. Wang, and Y. Yang, "Multiview consensus graph clustering," *TIP*, vol. 28, no. 3, pp. 1261–1270, 2018.
- [53] Y. Lin, Y. Gou, Z. Liu, B. Li, J. Lv, and X. Peng, "Completer: Incomplete multi-view clustering via contrastive prediction," in *CVPR*, 2021, pp. 11 174–11 183.
- [54] K. Hassani and A. H. Khasahmadi, "Contrastive multi-view representation learning on graphs," in *ICML*, 2020, pp. 4116–4126.
- [55] H. Binyuan, Z. Pengfei, and H. Qinghua, "Collaborative graph convolutional networks: Unsupervised learning meets semi-supervised learning," in *AAAI*, 2020.
- [56] C. Wang, S. Pan, R. Hu, G. Long, J. Jiang, and C. Zhang, "Attributed graph clustering: A deep attentional embedding approach," in *IJCAI*. AAAI Press, 2019, p. 3670–3676.
- [57] C. Tang, X. Liu, X. Zhu, E. Zhu, Z. Luo, L. Wang, and W. Gao, "Cgd: Multi-view clustering via cross-view graph diffusion," in *AAAI*, 2020.

APPENDIX

A. Overall Notations

The explanations of all notations are shown in Table VI.

B. Implementation Details

1) *Experimental Environments*: The experiments are conducted on a CentOS machine with a NVIDIA Tesla V100 SXM2 GPU and Cascade LakeP82 v6@2.4GHz CPU. CUDA version is 10.2 and PyTorch version is 1.11.0.

TABLE VI
OVERALL NOTATIONS.

\mathbf{A}^v	$\mathbf{A}^v \in \mathbb{R}^{n \times n}$, v -th view's adjacent matrix with self-loop.
\mathbf{D}^v	$\mathbf{D}^v = \sum_j a_{ij}^v$, degree matrix of \mathbf{A}^v .
$\tilde{\mathbf{A}}^v$	$\tilde{\mathbf{A}}^v = (\mathbf{D}^v)^{-1} \mathbf{A}^v$, normalized adjacent matrix.
$\check{\mathbf{A}}^v$	Reconstructed graph in generative process (Eq. (6)).
\mathbf{X}^v	$\mathbf{X}^v \in \mathbb{R}^{n \times d_v}$, v -th view's attributed features.
$\check{\mathbf{X}}^v$	Reconstructed features to calculate \mathcal{L}_r .
$\bar{\mathbf{X}}$	$\bar{\mathbf{X}} \in \mathbb{R}^{n \times d'}$, global features from all views' features.
\mathcal{G}^v	$\mathcal{G}^v = (\mathbf{X}^v, \mathbf{A}^v)$, v -th view's graph.
\mathbf{Z}^v	$\mathbf{Z}^v \in \mathbb{R}^{n \times D}$, v -th view's graph embedding.
$\bar{\mathbf{Z}}$	$\bar{\mathbf{Z}} \in \mathbb{R}^{n \times (V \cdot D)}$, final global embedding from $\{\mathbf{Z}^v\}_{v=1}^V$.
α	$\alpha \in \mathbb{R}^{n \times n}$ are the neurons used to obtain \mathbf{S} .
\mathbf{S}	$\mathbf{S} = \{s_{ij} \mid s_{ij} \sim \text{BinConcrete}(\alpha_{ij}, \tau)\}$.
$\hat{\mathbf{S}}$	$\hat{\mathbf{S}} \in \mathbb{R}^{n \times n}$, the variational consensus graph.
b^v	The belief of v -th graph, calculated from Eq. (13).
β_{ij}	$\beta_{ij} \in (0, 1]$, the parameter of Bernoulli distribution.
U	Sampled from Uniform distribution, $U \sim \text{Uniform}(0, 1)$.
ϕ'	The learnable parameters in $q_{\phi'}(\hat{\mathbf{S}} \mid \bar{\mathbf{X}})$.
η'	The learnable parameters in $q_{\eta'}(\alpha \mid \bar{\mathbf{X}})$.
η^v	The learnable parameters in $q_{\eta^v}(\mathbf{X}^v \mid \mathbf{Z}^v)$.
ϕ^v	The learnable parameters of f_v .
ρ	$\rho \geq 0$ is a hyper-parameter for belief b^v in Eq. (13).
τ	$\tau > 0$ is a hyper-parameter of temperature in Eq. (5).
<i>order</i>	A hyper-parameter of aggregation orders in Eq. (9).
\mathcal{L}_c	Task related loss for optimizing clustering results.
\mathcal{L}_r	Reconstruction loss for optimizing mutual information.
\mathcal{L}_E	ELBO for optimizing variational graph generator.
γ_c	A hyper-parameter to trade off the numerical value of \mathcal{L}_c .
γ_E	A hyper-parameter to trade off the numerical value of \mathcal{L}_E .

2) *Details of Global and Specific Graph Encoder*: Similar to the MLP f' , f_v also has three layers, the dimensions of *hidden* and *output* layers are chosen to be 512. The parameters ϕ^v are initialized with Kaiming, and *ReLU* is selected as the activation function.

3) *Details of Inference Process*: The variational consensus graph $\hat{\mathbf{S}}$ is generated through a f' from global features $\bar{\mathbf{X}}$. The instantiation of f' is an MLP, playing a role of encoder to extract the information from $\bar{\mathbf{X}}$. Specifically, f' consists of three layers, *i.e.*, *input* \rightarrow *hidden* \rightarrow *output*, and each layer follows a Dropout operation. In our model, we set the dimensions of both *hidden* and *output* layers as 512, drop rate of Dropout operation as 0.1 and all parameters of ϕ' are initialized with Xavier.

C. Details of Loss Functions

1) *Evidence Lower Bound Loss*: In the generative process, the decoder of $p_{\xi}^v(\mathbf{A}^v \mid \hat{\mathbf{S}}, \mathbf{X}^v)$ shares structure and parameters with f_v and ϕ^v . Finally, \mathbf{A}^v can be reconstructed through

$\sigma(\mathbf{Z}^v(\mathbf{Z}^v)^T)$, where $\sigma(\cdot)$ denotes *Sigmoid* function. Thus \mathcal{L}_E can be written as:

$$\mathcal{L}_E = - \sum_{v=1}^V H(\mathbf{A}^v, \check{\mathbf{A}}^v) + H(\hat{\mathbf{S}}) - \sum_{ij} \log \frac{1}{\beta_{ij}}. \quad (25)$$

2) *Lower Bound of Mutual Information Loss*: For the reconstruction of \mathbf{X}^v , \mathbf{Z}^v is fed into an MLP decoder, whose structure is the opposite of f_v . To reconstruct the global features $\bar{\mathbf{X}}$ to $\check{\bar{\mathbf{X}}}$, the obtained \mathbf{Q} is fed into an MLP decoder opposite of f' . Subsequently, the reconstruction losses \mathcal{L}_r^v and \mathcal{L}'_r for maximizing the lower bound of mutual information can be written as follows:

$$\begin{aligned} \mathcal{L}_r^v &= \sum_{v=1}^V H(\mathbf{X}^v, \check{\mathbf{X}}^v) \\ &= - \sum_{v=1}^V \sum_i [\mathbf{x}_i^v \log \check{\mathbf{x}}_i^v + (1 - \mathbf{x}_i^v) \log(1 - \check{\mathbf{x}}_i^v)], \end{aligned} \quad (26)$$

$$\begin{aligned} \mathcal{L}'_r &= H(\bar{\mathbf{X}}, \check{\bar{\mathbf{X}}}) \\ &= - \sum_i [\bar{\mathbf{x}}_i \log \check{\bar{\mathbf{x}}}_i + (1 - \bar{\mathbf{x}}_i) \log(1 - \check{\bar{\mathbf{x}}}_i)]. \end{aligned} \quad (27)$$

Finally, we can obtain our overall reconstruction loss \mathcal{L}_r :

$$\mathcal{L}_r = \sum_v \mathcal{L}_r^v + \mathcal{L}'_r \quad (28)$$

3) *Clustering Loss*: Clustering loss is specialized for clustering task [6, 27, 42], which encourages the assignment distribution of samples in a same cluster being more similar. Concretely, let $Q^v = \{q_{ij}^v\}$ be a soft assignment of i -th node to j -th cluster in v -th view, $\boldsymbol{\mu}^v \in \mathbb{R}^{c \times D}$ be c centroids of c clusters, q_{ij}^v is calculated by Student's t -distribution [43]:

$$q_{ij}^v = \frac{(1 + \|\mathbf{z}_i^v - \boldsymbol{\mu}_j^v\|^2)^{-1}}{\sum_j (1 + \|\mathbf{z}_i^v - \boldsymbol{\mu}_j^v\|^2)^{-1}}. \quad (29)$$

By sharpening the soft assignment q_{ij}^v , we can obtain its target distribution $\mathbf{P}^v = \{p_{ij}^v\}$:

$$p_{ij}^v = \frac{(q_{ij}^v)^2 / \sum_i q_{ij}^v}{\sum_j ((q_{ij}^v)^2 / \sum_i q_{ij}^v)}. \quad (30)$$

The clustering loss encourages soft assignment distribution Q^v to fit target distribution P^v by KL divergence, *i.e.*, $KL(P^v \parallel Q^v)$. In our multi-view clustering task, we assume that every view's soft distribution could fit the most correct target distribution, *i.e.*, the target distribution of global representation $\bar{\mathbf{Z}}$. Using \bar{P} and \bar{Q} denote the target and soft distribution of $\bar{\mathbf{Z}}$, the multi-view clustering loss could be improved as:

$$\mathcal{L}_c = \sum_{v=1}^V KL(\bar{P} \parallel Q^v) + KL(\bar{P} \parallel \bar{Q}). \quad (31)$$